Design of a Linear Paul Ion Trap

W. Jeffries, Old Dominion University
Advisor: Dr. Matt Grau, Old Dominion University

April 2024

Abstract

I outline the goals of my lab and report on the progress made in designing and building a linear Paul trap for trapped ion experiments involving barium and lutetium species. With a radial diameter of 2 mm, an axial size of 6 mm, operating with constant and oscillating voltages of 8 V and 80 V, respectively, oscillating at $2\pi \times 8$ MHz, I have found that the device should trap barium and lutetium ions. I also outline aspects of the trap design that cater to increasing observation signals.

1 Introduction

The observed imbalance of matter to antimatter in the universe goes directly against predictions of the standard model (SM) of particle physics, prompting investigations into beyond-standard-model (BSM) experiments and theories. Sakharov [1] determined two conditions for any quantum field theory that models an asymmetry in matter and antimatter formation: time-reversal (T) symmetry must be violated and the universe must evolve out of thermal equilibrium. By the CPT theorem, CPT symmetry (where charge-conjugation (C) refers to exchange of matter with antimatter and parity (P) refers to spatial inversion) is not violated, so T violation necessarily implies CP violation and vice versa. Though CP violation is present in the SM, it is too suppressed to account for observations. Generally, BSM theories include additional sources of CP violation either not found in the SM or altered from the predictions of the SM that would have an effect at lower energies, such as the electric dipole moments (EDMs) and magnetic quadrupole moments (MQMs) of charged particles and their composites [2, 3, 4, 5]. EDMs and MQMs offer a set of observables that complement current searches for BSM particles in modern colliders, with the benefit of being executed on the scale of table-tops and at lower costs than accelerator facilities, while providing mass constraints on BSM particles that are comparable to (and can exceed) the ability of the LHC [6].

Recently it was realized that atoms and heavy molecules are promising candidates in the search for CP-invariance violation [7]. Molecules in particular are useful as they offer experimental access to large effective electric fields (> 10GV/cm) [8]. Linear triatomic molecules offer several additional advantages over the isoelectronic diatomic molecules employed in recent EDM measurements [9, 10]: the ℓ-doubling effect gives a small energy gap between levels of opposite parity [8], meaning we can fully polarize them with relatively weak electric fields; the ℓ-doublet can suppress any systematic errors brought on by magnetic fields; and they can be laser-cooled [11]. Currently there are experiments planning to take advantage of these properties to perform high precision measurements of the MQM using ^{173}YbOH [12]. Due to their deformed nuclei, the atoms ^{175}Lu and ^{176}Lu have large MQMs, and recent calculations suggest that the CP-violating energy shift of ^{175}LuOH$^+$ and ^{176}LuOH$^+$ may be as much as a factor of 2 higher than that of ^{173}YbOH [11], making it a promising subject of study. These isotopologues are ionized to give them a similar electronic structure to that of YbOH while also allowing them to be easily trapped using ion trapping techniques.

Recent developments in the toolbox of trapped ion quantum information experiments have resulted in high contrast measurements with low dead times [13]. I aim to utilize techniques such as quantum logic spectroscopy to investigate LuOH$^+$. Trapping has a number of benefits that contribute to high-precision results, including the ease of cooling and trapping and the high fidelity associated with detection due to the long interrogation times it permits. Additionally, quantum-information-style ion trap experiments offer easy scalability, allowing us to eventually build an experiment that simultaneously treats hundreds of trapped molecular ions [14].

In this paper, I will discuss the mathematical considerations involved in trapping ions and building a functioning ion trap. I will discuss how these considerations were incorporated into our ion trap design, and I will discuss how these considerations will aid in performing the experiments outlined above.

2 Trapping Ions

While it is possible to confine neutral atoms using such apparatuses as the magneto-optical trap or optical tweezers (see [15], Ch 10), the trapping of ions by electric fields offers stronger confinement at less cost (see [15], Ch 12). Earnshaw's theorem (see [16], Ch 3) states that a point charge cannot be held at equilibrium solely by an electrostatic interaction, however one can circumvent this theorem using a time-varying force; considering the two-dimensional case, we can produce a field which is confining along one direction and non-confining along another direction, e.g. the quadrupole field depicted in Fig. 1a. A positive charge will move in the direction of the arrows of the field. As the charge begins to move in that direction, we can invert the field with some frequency ω_{rf} which will invert the sign of the field, causing the particle to change its trajectory into the new direction of the arrows. This oscillation can cause a charge to stay localized to a small region near the center of the quadrupole field. An example of this kind of motion is depicted by the blue trajectory in Fig. 1a.

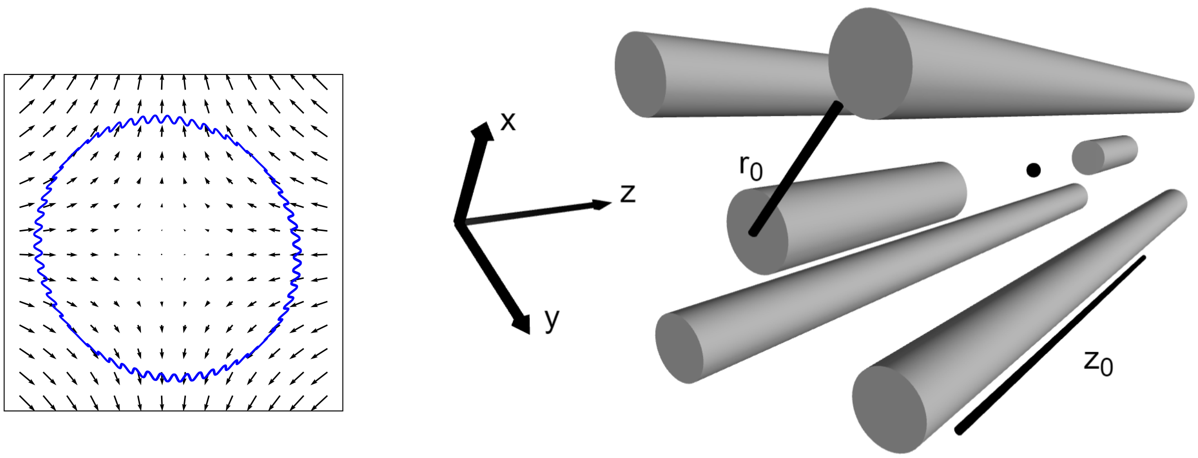

(a) (b)

Figure 1: (a) A 2-dimensional quadrupole field, with a sample trajectory (blue). (b) A linear Paul trap.

A linear Paul trap consists of six electrodes arranged in a configuration like that of Fig. 1b. The four long electrodes produce the quadrupole field in the radial (xy) directions, while the two short electrodes, called "endcaps," produce another quadrupole field that confines motion along the axial (z) direction. We put a voltage of V_{dc} on each endcap and $2V_{\mathrm{rf}}\cos(\omega_{\mathrm{rf}}t)$ across two diagonal electrodes (grounding the remaining electrodes). Assuming the oscillation is not too rapid (say at a radiofrequency of less than $2\pi \times 100$MHz), the magnetic fields produced by the changing electric field may be neglected. In general, the total field produced by this configuration requires a multipole expansion; however the field along the central axis of the trap can be approximated to lowest order by the quadrupole field

$$\begin{aligned}\Phi(x,y,z,t) =& \frac{V_{\mathrm{dc}}}{2z_0^2}\left(-x^2-y^2+2z^2\right)+ \\ & \frac{V_{\mathrm{rf}}}{2r_0^2}\cos(\omega_{\mathrm{rf}}t)\left(x^2-y^2\right),\end{aligned} \tag{1}$$

where z_0 is the distance from the center of the trap to the endcaps and r_0 is the shortest distance from the trap axis to the electrodes.

The equations of motion (EOMs) for an atomic ion of mass m and charge Ze under the influence of the field in Eq. 1 are

$$\begin{aligned}\ddot{x} + \frac{Ze}{m}\left(-\frac{V_{\mathrm{dc}}}{z_0^2} + \frac{V_{\mathrm{rf}}}{r_0^2}\cos(\omega_{\mathrm{rf}}t)\right)x = 0,\\ \ddot{y} + \frac{Ze}{m}\left(-\frac{V_{\mathrm{dc}}}{z_0^2} - \frac{V_{\mathrm{rf}}}{r_0^2}\cos(\omega_{\mathrm{rf}}t)\right)y = 0,\\ \ddot{z} + \frac{Ze}{m}\left(2\frac{V_{\mathrm{dc}}}{z_0^2}\right)z = 0,\end{aligned} \tag{2}$$

though it is customary to introduce some substitutions to facilitate simpler expressions. First, let $\xi = \frac{\omega_{\mathrm{rf}}t}{2}$ $\left(\Rightarrow \frac{\mathrm{d}^2}{\mathrm{d}t^2} = \frac{\omega_{\mathrm{rf}}^2}{4}\frac{\mathrm{d}^2}{\mathrm{d}\xi^2}\right)$ and let

$$
\begin{aligned}
a_x &= -\frac{4Ze}{m\omega_{\rm rf}^2}\frac{V_{\rm dc}}{z_0^2}, & a_y &= -\frac{4Ze}{m\omega_{\rm rf}^2}\frac{V_{\rm dc}}{z_0^2}, & a_z &= \frac{8Ze}{m\omega_{\rm rf}^2}\frac{V_{\rm dc}}{z_0^2}, \\
q_x &= -\frac{2Ze}{m\omega_{\rm rf}^2}\frac{V_{\rm rf}}{r_0^2}, & q_y &= \frac{2Ze}{m\omega_{\rm rf}^2}\frac{V_{\rm rf}}{r_0^2}, & q_z &= 0.
\end{aligned} \tag{3}
$$

Then Eqs. 2 become

$$
\frac{\mathrm{d}^2 x_i}{\mathrm{d}\xi^2} + (a_i - 2q_i\cos(2\xi))\,x_i = 0, \tag{4}
$$

for $i = x, y, z$. Eq. 4 is called Mathieu's equation, whose solutions, the Mathieu functions, are already well understood [17, 18, 19].

We say that the ion's motion is "stable" if the trajectory is bounded in the limit that $\xi \to \infty$. To determine whether an ion is stable in our model of a trap for given a_i and q_i ($i = x, y, z$), we can evaluate the solutions of the EOMs and check if they exceed some minimum allowed distance from the center of the trap. We can produce a plane of pairs (q_i, a_i), coloring in points that correspond to stable trajectories in black; this produces a "stability diagram" (also known as a Ince-Strutt diagram) like that found in Fig. 2a. Initial conditions have no influence on the stability of a solution to Mathieu's equation due to its linearity, meaning we can produce these stability diagrams without the need to specify initial conditions.

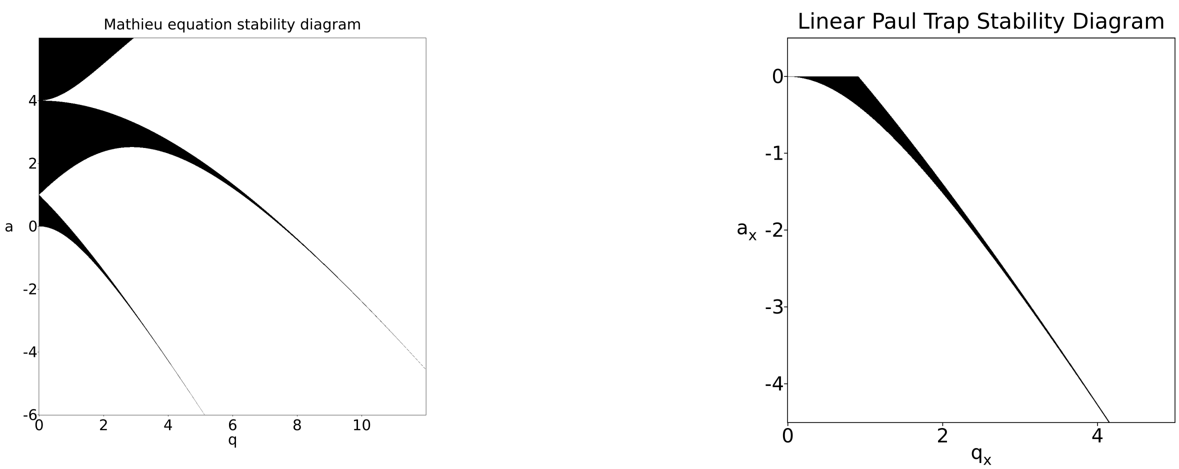

(a) (b)

Figure 2: (a) The stability diagram for the Mathieu equation. Black regions are stable regions and white regions are unstable regions. (b) The first stability region for the linear Paul trap, in terms of x-directed stability. Black regions are stable regions and white regions are unstable regions.

While Fig. 2a is *the* stability diagram for the Mathieu equation, the choice in the geometry of an ion trap will couple the Mathieu parameters (q, a) for the x, y, and z motion. In particular, from Eqs. 3 we find that

$$
a_z = -2a_x = -2a_y; \quad q_y = -q_x; \quad q_z = 0q_x,
$$

and thus that a stability diagram that applies to the motion in both x and y is found by taking the intersections of the stable regions in Fig. 2a with the stable regions flipped about the a_x axis for the y-directed motion, and with the stable regions along the $q_x = 0$ line for the z-directed motion. The result is shown in Fig. 2b. Recall from Eq. 4 that the EOM in z is really that of the simple harmonic oscillator with frequency $\omega_z = \sqrt{a_z}$, which only admits negative eigenvalues, giving stability along z for all $a_x \leq 0$.

In the limit of small a_i and q_i, the motion can be reasonably approximated using a few terms in a Fourier series [20]

$$\begin{aligned} x_i(t) &\approx 2A\left[-\frac{q_i}{4}\cos\left(\left(\frac{\beta_i}{2}-1\right)\omega_{\rm rf}t\right)+\right. \\ &\qquad \left.\cos\left(\frac{\beta_i}{2}\omega_{\rm rf}t\right)-\frac{q_i}{4}\cos\left(\left(\frac{\beta_i}{2}+1\right)\omega_{\rm rf}t\right)\right] \\ &= 2A\cos\left(\beta_i\frac{\omega_{\rm rf}}{2}t\right)\left[1-\frac{q_i}{2}\cos\left(\omega_{\rm rf}t\right)\right], \end{aligned}$$

where $i = x, y, z$ and $\beta_i \approx \sqrt{a_i + q_i^2/2}$. The trajectory features motion of two frequencies, $\beta_i\omega_{\rm rf}/2$ and $\omega_{\rm rf}$, called the "secular motion" and the "micromotion," respectively.

The regions of stability in Fig. 2a are numbered according to the order they are encountered as we go up the a_x axis (i.e. "first," "second," etc.). By accounting for the motion along all three directions, only the portions of the stability regions that rest below the $a_x = 0$ line remain. The second stability region encounters this line around $q_x \approx 7.5$; it is difficult to produce rf fields that correspond to q_x in this range, so ion trappers typically aim for the first stability region which is closer to the $0 \leq q_x \lesssim 0.908$ range for small a_x.

3 Ion Trap Design

While there are many geometries that can trap a given ion, we are often limited by practical limitations such as the achievable voltages and frequencies of our experimental equipment. As a basic guideline, we seek to find values in the following ranges:

- $|a_x| \gtrsim 0$, and $a_x < 0$,
- $-0.15 \lesssim q_x \lesssim 0$,
- $\omega_{\rm sec}$ as large as possible.

My lab is limited to values in the following ranges:

- $|V_{\rm dc}| \lesssim 10$V,
- $V_{\rm rf} \lesssim 100$V,
- $\omega_{\rm rf} \lesssim 2\pi \times 20$MHz.

Our choice of r_0 and z_0 will serve to produce stable (q, a) as well as sufficiently large secular frequency. A large secular frequency is necessary to put the ion in the Lamb Dicke regime, which is a regime in which the coupling between the ion's internal qubit states and motional states is sufficiently small such that any transitions that change the motional quantum number $\Delta n > 1$ are strongly suppressed [20]. The Lamb-Dicke regime is characterized by the Lamb-Dicke parameter $\eta \propto (\beta_i\omega_{\rm rf}/2)^{-1/2}$ when $\eta \ll 1$, meaning the secular frequency must be large.

In the interest of producing a large secular motion frequency, we aim to make $\omega_{\rm rf}$ large: let $\omega_{\rm rf} = 2\pi \times 8$MHz. This choice restricts $V_{\rm dc}$ and $V_{\rm rf}$. Letting $V_{\rm dc} = 8$V and $V_{\rm rf} = 80$V, the optimal values of a_x and q_x that both trap an ion and produce a large secular frequency are $r_0 = 0.5$mm, $z_0 = 3$mm. Assuming a singly ionized particle ($Ze = 1$e), then the (q_x, a_x) coordinates of ^{137}Ba$^+$, ^{138}Ba$^+$, ^{175}Lu$^+$, ^{176}Lu$^+$, ^{175}LuOH$^+$, and ^{176}LuOH$^+$ are given in Table 1, along with the corresponding secular frequencies of motion in the z, x, and y directions.

	q_x	a_x	$\frac{\omega_z}{2\pi}$(kHz)	$\frac{\omega_{x,y}}{2\pi}$(kHz)
$^{137}Ba^+$	-0.0892	-0.000911	178	219
$^{138}Ba^+$	-0.0886	-0.000984	177	217
$^{175}Lu^+$	-0.0698	-0.000776	158	163
$^{176}Lu^+$	-0.0694	-0.000772	157	162
$^{175}LuOH^+$	-0.0636	-0.000707	150	145
$^{176}LuOH^+$	-0.0633	-0.000704	150	144

Table 1: Mathieu parameters and motional frequencies for $^{137}Ba^+$, $^{138}Ba^+$, $^{175}Lu^+$, $^{176}Lu^+$, $^{175}LuOH^+$, and $^{176}LuOH^+$.

One of the simplest linear Paul trap designs employs blade-like electrodes which offer greater optical access (over cylindrical and hyperbolic electrodes) to the center of the trap without sacrificing the origin-to-electrode distance r_0 [21]. The simplest blade design possesses planar symmetry, and the four blades are arranged at 45° from the vertical and horizontal axes in the trap (see Fig. 3a); however, a linear Paul trap often reserves the horizontal plane for laser-addressing, while the vertical axis is reserved for imaging. Since the lasers in the horizontal plane often have a beam waist of no more than 0.75mm, we are free to reduce the angle between the blades and the horizontal plane and increase the angle with the vertical axis without sacrificing laser access. Additionally, we can slightly reduce the distance of the blades to the horizontal plane. This increases the solid angle available for photon collection in the optical system. In a similar vein, it is common to design asymmetric blades that further cater to our desire to maximize the angle of optical access (see Fig. 3b). The blades have an internal angle of 30° and are arranged 42° from the vertical axis and 18° from the horizontal axis.

To compare the collection efficiency of these two configurations, we can look at the fraction of a sphere that is subtended by a cone formed by the angle from the vertical axis to the first point of contact with the blades. Assuming the length of the side of the blades facing the vertical axis is $d = 4.918$mm and the interior angles are 30°, and recalling that the asymmetric blades are slightly displaced toward the horizontal plane, we find the angle from the vertical is 30.855° and 43.660° for the symmetric and asymmetric arrangement, respectively, which amounts to 7.076% and 13.828% of the solid angle of a sphere (as a reminder, 50% would be the "ideal" case). This corresponds to an increase in collection efficiency by a factor of 1.95.

(a) (b)

Figure 3: (a) A simple blade arrangement. (b) An optimized blade arrangement.

Similar ideas can be applied to the endcaps to increase their proximity to the ions (decreasing z_0 and decreasing the necessary $V_{\rm dc}$ of the trap) without sacrificing optical efficiency. Additionally, a 1mm hole is drilled along the axis of the endcaps to offer optical access for a laser (see Fig. 4a).

(a) (b)

Figure 4: (a) Endcap. (b) Macor mount.

The blades and endcaps are secured to two insulating mounts that isolate each conductor and fix their positions in the trap. The mounts are made of Macor, a machinable vacuum-safe ceramic. Its machinability allowed us to cut it into a shape that maximizes accessibility to ions from lasers (see Fig. 4b).

Since the blades and endcaps are close to the center of the trap, they must be non-porous materials, such as stainless steel 304 (SS304) or oxygen-free electronic (OFE) copper, to avoid outgasing in the vacuum. The blades are made of SS304 and the endcaps are OFE copper. The Macor mounts insulate the electrodes and are non-porous to prevent outgasing complications near the ions. The configured trap can be found in Fig. 5.

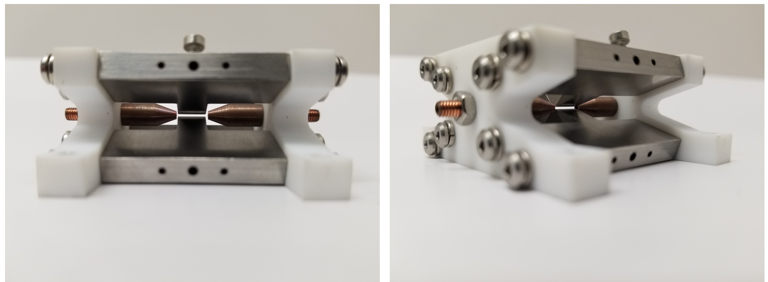

Figure 5: The assembled ion trap.

4 Summary

I have given an outline of the ideas we must consider when designing an ion trap for precision quantum information experiments on $^{137}Ba^+$, $^{138}Ba^+$, $^{175}Lu^+$, $^{176}Lu^+$, $^{175}LuOH^+$, and $^{176}LuOH^+$. With this trap, I aim to perform experiments on Ba^+ that will aid in the development of quantum information techniques that can be directly implemented on Lu^+ and $LuOH^+$ to perform high-precision CP-violation experiments, with expected results comparable to contemporary experiments currently underway in groups such as JILA. Along the way, I aim to resolve the branching ratios of Ba^+ isotopes and compare with recent *ab initio* calculations performed by [22], which will simultaneously address a recent disparity between experiment and theory and allow our lab to gain experience with some of the techniques that will be involved in a CP-violation experiment.

References

[1] Andrei D Sakharov. Violation of CP invariance, C asymmetry, and baryon asymmetry of the universe. *Soviet Physics Uspekhi*, 34(5):392, may 1991.

[2] Maxim Pospelov and Adam Ritz. Ckm benchmarks for electron electric dipole moment experiments. *Physical Review D*, 89(5), March 2014.

[3] Yasuhiro Yamaguchi and Nodoka Yamanaka. Large long-distance contributions to the electric dipole moments of charged leptons in the standard model. *Physical Review Letters*, 125(24), December 2020.

[4] Yasuhiro Yamaguchi and Nodoka Yamanaka. Quark level and hadronic contributions to the electric dipole moment of charged leptons in the standard model. *Physical Review D*, 103(1), January 2021.

[5] V. V. Flambaum, D. DeMille, and M. G. Kozlov. Time-reversal symmetry violation in molecules induced by nuclear magnetic quadrupole moments. *Physical Review Letters*, 113(10), September 2014.

[6] William B. Cairncross and Jun Ye. Atoms and molecules in the search for time-reversal symmetry violation. *Nature Reviews Physics*, 1(8):510–521, 2019.

[7] P. G. H. Sandars. Measurability of the proton electric dipole moment. *Phys. Rev. Lett.*, 19:1396–1398, Dec 1967.

[8] Ivan Kozyryev and Nicholas R. Hutzler. Precision measurement of time-reversal symmetry violation with laser-cooled polyatomic molecules. *Phys. Rev. Lett.*, 119:133002, Sep 2017.

[9] V. Andreev, D. G. Ang, D. DeMille, J. M. Doyle, G. Gabrielse, J. Haefner, N. R. Hutzler, Z. Lasner, C. Meisenhelder, B. R. O'Leary, C. D. Panda, A. D. West, E. P. West, and X. Wu. Improved limit on the electric dipole moment of the electron. *Nature*, 562(7727):355–360, 2018.

[10] William B. Cairncross, Daniel N. Gresh, Matt Grau, Kevin C. Cossel, Tanya S. Roussy, Yiqi Ni, Yan Zhou, Jun Ye, and Eric A. Cornell. Precision measurement of the electron's electric dipole moment using trapped molecular ions. *Phys. Rev. Lett.*, 119:153001, Oct 2017.

[11] D. E. Maison, L. V. Skripnikov, V. V. Flambaum, and M. Grau. Search for CP-violating nuclear magnetic quadrupole moment using the $LuOH^+$ cation. *The Journal of Chemical Physics*, 153(22), December 2020.

[12] D. E. Maison, L. V. Skripnikov, and V. V. Flambaum. Theoretical study of ^{173}YbOH to search for the nuclear magnetic quadrupole moment. *Phys. Rev. A*, 100:032514, Sep 2019.

[13] Yan Zhou, Joshua O. Island, and Matt Grau. Quantum logic control and precision measurements of molecular ions in a ring trap – a new approach for testing fundamental symmetries, 2023.

[14] S. Jain, J. Alonso, M. Grau, and J. P. Home. Scalable arrays of micro-penning traps for quantum computing and simulation. *Phys. Rev. X*, 10:031027, Aug 2020.

[15] Christopher Foot. *Atomic physics*. Oxford University Press, USA, 2005.

[16] David J Griffiths. *Introduction to electrodynamics*. Pearson, 2013.

[17] Émile Mathieu. Mémoire sur le mouvement vibratoire d'une membrane de forme elliptique. *Journal de Mathématiques Pures et Appliquées*, 13:137–203, 1868.

[18] N. W. McLachlan. *Theory and Application of Mathieu Functions*. Oxford University Press, 1947.

[19] E. L. Ince. *Ordinary Differential Equations*. Longmans, Green and Company Limited, 1927.

[20] D. Leibfried, R. Blatt, C. Monroe, and D. Wineland. Quantum dynamics of single trapped ions. *Rev. Mod. Phys.*, 75:281–324, Mar 2003.

[21] K. Deng, H. Che, Y. Lan, Y. P. Ge, Z. T. Xu, W. H. Yuan, J. Zhang, and Z. H. Lu. Design of blade-shaped-electrode linear ion traps with reduced anharmonic contributions. *Journal of Applied Physics*, 118(11):113106, 09 2015.

[22] K. J. Arnold, S. R. Chanu, R. Kaewuam, T. R. Tan, L. Yeo, Zhiqiang Zhang, M. S. Safronova, and M. D. Barrett. Measurements of the branching ratios for $6P_{1/2}$ decays in $^{138}Ba^+$. *Phys. Rev. A*, 100:032503, Sep 2019.